Ring polymer quantization of the photon field in polariton chemistry

Sutirtha N. Chowdhury, Arkajit Mandal, and 🆔 Pengfei Huo

Ring polymer quantization of the photon field in polariton chemistry

View Online   Export Citation   CrossMark

Sutirtha N. Chowdhury, Arkajit Mandal, and Pengfei Huo[a] (iD)

AFFILIATIONS

Department of Chemistry, University of Rochester, 120 Trustee Road, Rochester, New York 14627, USA

Note: This paper is part of the JCP Special Topic on Polariton Chemistry: Molecules in Cavities and Plasmonic Media.
[a]Author to whom correspondence should be addressed: pengfei.huo@rochester.edu

ABSTRACT

We use the ring polymer (RP) representation to quantize the radiation field inside an optical cavity to investigate polariton quantum dynamics. Using a charge transfer model coupled to an optical cavity, we demonstrate that the RP quantization of the photon field provides accurate rate constants of the polariton mediated electron transfer reaction compared to Fermi's golden rule. Because RP quantization uses extended phase space to describe the photon field, it significantly reduces the computational costs compared to the commonly used Fock state description of the radiation field. Compared to the other quasi-classical descriptions of the photon field, such as the classical Wigner based mean-field Ehrenfest model, the RP representation provides a much more accurate description of the polaritonic quantum dynamics because it alleviates the potential quantum distribution leakage problem associated with the photonic degrees of freedom (DOF). This work demonstrates the possibility of using the ring polymer description to treat the quantized radiation field in polariton chemistry, offering an accurate and efficient approach for future investigations in cavity quantum electrodynamics.

Published under license by AIP Publishing. https://doi.org/10.1063/5.0038330

I. INTRODUCTION

Coupling molecules to the quantized radiation field inside an optical cavity creates a set of new photon-matter hybrid states, so-called polaritons. These light–matter hybrid polaritons have shown great promise to control chemical reactivities[1–7] in a general way by tuning the fundamental properties of photons and provides a new paradigm for enabling chemical transformations that can profoundly impact catalysis, energy production, and the field of chemistry at large. Theoretical investigations have played a crucial role in unraveling the fundamental principles of polariton chemistry.[4–20] Despite encouraging progress, accurately and efficiently simulating these polariton quantum dynamics processes opens a brand new challenge in theoretical chemistry.

In previous works of polariton chemistry, the cavity photon field has been treated quantum mechanically through Fock states,[8,9,12,13,15,18,19] grid points,[4,11,21] coherent states,[7] and polarized Fock states.[22] These approaches provide an accurate description of the quantum light–matter interactions. They are, however, computationally demanding as they involve the full quantum description

of the radiation modes and are often limited in terms of how many modes can be explicitly quantized.

The similarity (or even the isomorphism) between the vibrational quantization of nuclei in molecules and the photonic quantization of the radiation mode inside the cavity has inspired the quasi-classical description of the photon field. In fact, quasi-classical quantization (in the action-angle quasi-classical description) of the photon field has been historically used to treat molecule-laser field interaction by Miller and co-workers.[23,24] A recent example of the quasi-classical description of the radiation mode in cavity quantum electrodynamics (QED) includes the classical Wigner based mean-field Ehrenfest model[25–27] as well as the symmetric quasi-classical window approach.[27,28] Here, we refer to the classical Wigner based mean-field Ehrenfest model as an approach that samples the nuclear or photonic degrees of freedom (DOFs) through initial Wigner quantum distribution and then propagates them through the classical equation of motion. In the following, we refer to this classical Wigner based mean-field Ehrenfest model as the classical Wigner model for simplicity. These quasi-classical approaches can significantly reduce the computational cost due to

the quasi-classical treatment of the photon field. However, the classical Wigner model[25,26] is expected to cause incorrect quantum dynamics due to the leakage of the zero-point energy (ZPE).[29–31] Note that when coupling molecules with the *classical* radiation field (through the description from the classical Maxwell equations), the detailed balance has been enforced in the recent Ehrenfest+R approach.[32] With its current implementation, on the other hand, Ehrenfest+R is limited to the weak light–matter interactions (that causes the exponential decay of the excited state population) through a phenomenologically introduced spontaneous decay channel.

These shortcomings of the quasi-classical treatment can be readily addressed with the recently developed state-dependent ring polymer molecular dynamics (RPMD) approaches.[33–38] These approaches are based upon the imaginary-time path-integral description of the quantum DOF in the extended phase space.[39–44] The classical evolution in RPMD (for a thermal-equilibrium system) preserves its initial quantum distribution captured by the ring polymer Hamiltonian, and it is free of the zero-point energy leaking problem.[29,44] With the recent development of state-dependent RPMD approaches,[33–38] one can accurately capture both non-adiabatic electronic transitions in molecular systems while explicitly quantizing either the nuclear DOF or even the photonic mode through the ring polymer description. The ring polymer has been previously used to quantize the electron,[45–48] proton[49,50] and hydride,[51] hydrogen and muonium atoms,[52] molecular hydrogen,[53] helium,[40] coupled electron and proton,[54,55] as well as coupled electron and hole.[56]

In this work, we quantize the photon field with the ring polymer description and simulate the polariton mediated electron transfer (PMET) reaction through the non-adiabatic RPMD (NRPMD) approach.[31,33,38] To the best of our knowledge, this is the first numerical example of using the ring polymer representation[40,41,44] to quantize the cavity photon field. We demonstrate that the ring polymer quantization of the photon field provides an accurate polaritonic quantum dynamics of the molecule-cavity hybrid system, compared to the quasi-classical description with the classical Wigner model. We further provide an interesting interpretation of the influence from the cavity field on the molecule as a fluctuating (Peierls-type) coupling that facilitates the charge transfer.

II. THEORETICAL APPROACH

We start with the Pauli–Fierz (PF) non-relativistic QED Hamiltonian[13,20,21,57,58] to describe the molecular system $\hat{H}_m$ coupled to the radiation field $\hat{H}_P = (\hat{a}^\dagger \hat{a} + \frac{1}{2})\hbar\omega_c$ inside an optical cavity under the long-wavelength limit.[20] A brief derivation of this Hamiltonian is provided in the Appendix. The PF Hamiltonian is

$$\hat{H}_{PF} = \hat{H}_m + \left(\hat{a}^\dagger \hat{a} + \frac{1}{2}\right)\hbar\omega_c + \boldsymbol{\chi}\cdot\hat{\boldsymbol{\mu}}(\hat{a}^\dagger + \hat{a}) + \frac{(\boldsymbol{\chi}\cdot\hat{\boldsymbol{\mu}})^2}{\hbar\omega_c}$$

$$= \hat{H}_m + \frac{1}{2}\hat{P}_c^2 + \frac{1}{2}\omega_c^2\left(\hat{Q}_c + \sqrt{\frac{2}{\hbar\omega_c^3}}\boldsymbol{\chi}\cdot\hat{\boldsymbol{\mu}}\right)^2, \quad (1)$$

where $\hat{a}^\dagger$ and $\hat{a}$ are the photonic creation and annihilation operator, respectively, and $\hat{Q}_c = \sqrt{\hbar/2\omega_c}(\hat{a}^\dagger + \hat{a})$ and $\hat{P}_c = i\sqrt{\hbar\omega_c/2}(\hat{a}^\dagger - \hat{a})$ are the photon field coordinate and momentum operators, with ω_c as the photon frequency inside the cavity. Furthermore, $\boldsymbol{\chi} = \sqrt{\frac{\hbar\omega_c}{2\varepsilon_0\mathcal{V}}}\hat{\mathbf{e}}$ characterizes the light–matter interaction. The unit vector $\hat{\mathbf{e}}$ is along the field polarization direction, $\mathcal{V}$ is the quantization volume for the cavity photon field, and ε_0 is the permittivity inside the cavity. Finally, $\hat{\boldsymbol{\mu}}$ is the total molecular dipole operator (for both electrons and nuclei). $\hat{H}_{PF}$ is a pure real Hamiltonian, and the photonic DOF can be viewed as an additional "nuclear" DOF, hence computationally treated in that way. In this work, we only consider a single cavity mode to clearly demonstrate the accuracy of various theoretical treatments of the photon field. In reality, the matter will couple to multiple modes inside the cavity.[25–27,59]

The central idea of this paper is to treat the photonic DOF in Eq. (1) as classical variables, i.e., $\hat{Q}_c \to Q_c$ and $\hat{P}_c \to P_c$, then quantizing them through the ring polymer description.[40,41,44] More specifically, we treat both the nuclear DOF $\mathbf{R}$ and the photonic DOF Q_c on an equal footing and denote the "nuclear" DOF in the hybrid system as $\mathbf{X} = \{\mathbf{R}, Q_c\}$, with the corresponding momenta $\boldsymbol{\Pi} = \{\mathbf{P}, P_c\}$. For a given diabatic Hamiltonian $\hat{H} = \hat{\mathbf{T}} + \hat{V}_0(\hat{\mathbf{X}}) + \sum_{ij} V_{ij}(\hat{\mathbf{X}})|i\rangle\langle j|$, the NRPMD approach[31,33,38] suggests that there is an isomorphic Hamiltonian[31,33,34] as follows:

$$H_\mathcal{N} = \sum_{\alpha=1}^\mathcal{N} \frac{1}{2\mathbf{M}}\boldsymbol{\Pi}_\alpha^2 + V_0(\mathbf{X}_\alpha) + \frac{\mathbf{M}}{2\beta_\mathcal{N}^2\hbar^2}(\mathbf{X}_\alpha - \mathbf{X}_{\alpha-1})^2$$

$$+ \frac{1}{2\hbar}\sum_{ij} V_{ij}(\mathbf{X}_\alpha)\left([\mathbf{q}_\alpha]_i[\mathbf{q}_\alpha]_j + [\mathbf{p}_\alpha]_i[\mathbf{p}_\alpha]_j - \delta_{ij}\hbar\right), \quad (2)$$

where the coordinate $\mathbf{X}$ (with the corresponding mass $\mathbf{M}$) is quantized through the extended phase space description with $\mathcal{N}$ copies (the number of the imaginary time slices) $\{\mathbf{X}_\alpha\}$ of the original coordinate that are harmonically coupled to each other. This is commonly referred to as the ring polymer. The diabatic states $\{|i\rangle\}$ are mapped onto a set of mapping oscillators $\{q_i, p_i\}$ through the Meyer–Miller–Stock–Thoss (MMST) formalism,[60,61] which are then extended to $\mathcal{N}$ copies $\{[\mathbf{q}_\alpha]_i, [\mathbf{p}_\alpha]_i\}$ as well in the NRPMD Hamiltonian.[31,34,38] The above Hamiltonian provides accurate non-adiabatic quantum dynamics and, at the same time, explicitly captures nuclear quantum effects, as demonstrated in several model systems in previous studies.[31,33,38]

In the NRPMD quantum dynamics approach,[31,33,38] the classical trajectories are propagated according to the Hamilton's equation of motion associated with $H_\mathcal{N}$ in Eq. (2). The motion of the "nuclei" ($\mathbf{X}$) is governed by $\dot{\boldsymbol{\Pi}}_\alpha = -\nabla_{\mathbf{X}_\alpha}H_\mathcal{N}$, with the detailed equation of motion as follows:

$$\dot{\boldsymbol{\Pi}}_\alpha = -\frac{\mathbf{M}}{\beta_\mathcal{N}^2\hbar^2}(2\mathbf{X}_\alpha - \mathbf{X}_{\alpha+1} - \mathbf{X}_{\alpha-1}) - \nabla_{\mathbf{x}_\alpha}V_0(\mathbf{X}_\alpha)$$

$$- \frac{1}{2\hbar}\sum_{ij}\nabla_{\mathbf{x}_\alpha}V_{ij}(\mathbf{X}_\alpha)\left([\mathbf{q}_\alpha]_i[\mathbf{q}_\alpha]_j + [\mathbf{p}_\alpha]_i[\mathbf{p}_\alpha]_j - \delta_{ij}\hbar\right). \quad (3)$$

The bead-specific mapping variables $[\mathbf{q}_\alpha]_i$ and $[\mathbf{p}_\alpha]_i$ are propagated based on the following Hamilton's equations of motion:

$$[\dot{\mathbf{q}}_\alpha]_i = \frac{\partial H_\mathcal{N}}{\partial [\mathbf{p}_\alpha]_i} = \frac{1}{\hbar} \sum_j V_{ij}(\mathbf{X}_\alpha)[\mathbf{p}_\alpha]_j, \quad (4)$$

$$[\dot{\mathbf{p}}_\alpha]_i = -\frac{\partial H_\mathcal{N}}{\partial [\mathbf{q}_\alpha]_i} = -\frac{1}{\hbar} \sum_j V_{ij}(\mathbf{X}_\alpha)[\mathbf{q}_\alpha]_j. \quad (5)$$

Below, we present the model system used in this work, the analytical rate constant expression used as the benchmark of the quantum results, details of our NRPMD quantum dynamics simulations, and alternative theoretical descriptions for the photon field.

A. Model system

Using an optical cavity to manipulate electron transfer reactions[8,58,62,63] has gained an increasing interest in polariton chemistry. It has been shown that coupling to a quantized radiation mode can significantly enhance or suppress the electron transfer (ET) rate constants by using photon-dressed reactive channels.[8,58,62,63] Accurately and efficiently simulating the polariton mediated electron transfer (PMET) reaction, one of the most fundamental polariton chemical reactions, will significantly advance our ability to theoretically investigate molecular cavity quantum electrodynamics.

In this paper, we consider a donor–acceptor charge transfer system coupled to a single radiation mode inside the cavity.[58] The charge transfer molecular Hamiltonian is

$$\hat{H}_m = \frac{\hat{P}_s^2}{2M_s} + \sum_i U_i |i\rangle\langle i| + V_{DA}(|D\rangle\langle A| + |A\rangle\langle D|)$$
$$+ \sum_i \frac{1}{2} M_s \omega_s^2 (R_s - R_i^0)^2 |i\rangle\langle i| + \hat{H}_{sb}, \quad (6)$$

where $|i\rangle \in \{|D\rangle, |A\rangle\}$ is the diabatic donor or acceptor state and $\hat{T}_s = \hat{P}_s^2/2M_s$ represents the kinetic energy operator of the solvent coordinate R_s with mass M_s and frequency ω_s. Furthermore, U_i is the constant diabatic energy associated with the state $|i\rangle$, with $U_D = 0$ and $U_A = -\varepsilon$, and V_{DA} is the constant diabatic electronic coupling. The driving force (bias) ΔG of the reaction is $\Delta G = U_A - U_D = -\varepsilon$, and $\lambda = \frac{1}{2} M_s \omega_s^2 (R_A^0 - R_D^0)^2$ is the solvent reorganization energy. Furthermore, we take $R_D^0 = 0$ and $R_A^0 = \sqrt{2\lambda/f_0}$, where f_0 is the force constant, which is related to the solvent frequency $\omega_s = \sqrt{f_0/M_s}$. Throughout this study, we use the solvent reorganization energy of $\lambda = 650$ meV. Finally, $\hat{H}_{sb}$ describes the interaction between the solvent mode R_s and a dissipative bath as follows:

$$\hat{H}_{sb} = \sum_k \frac{P_k^2}{2M_k} + \frac{M_k \omega_k^2}{2}\left(R_k - \frac{c_k}{M_k \omega_k^2} R_s\right)^2, \quad (7)$$

where R_k represents the k_{th} bath mode with a conjugate momentum P_k and a mass $M_k = M_s$. The coupling constant c_k and the frequency ω_k are characterized by an Ohmic spectral density

$J(\omega) = \frac{\pi}{2} \sum_k \frac{c_k^2}{M_k \omega_k} \delta(\omega - \omega_k) = \eta \omega e^{-\omega/\omega_b}$ with a characteristic frequency $\omega_b = 9.5$ meV and a friction constant η. The details of the bath discretization and all the above parameters are provided in the supplementary material.

We further assume that the transition dipole and the permanent dipoles of the molecule are constants, i.e., not a function of the solvent coordinate.[62] We find that within the light–matter coupling strength considered in this work, the presence of the permanent dipoles does not impact the polariton quantum dynamics because these permanent dipoles only couple the states that are energetically off-resonance, for example, $|D, n\rangle$ and $|D, n \pm 1\rangle$. Hence, we completely ignore the permanent dipoles in our quantum dynamics simulations presented in the main text. In the supplementary material, we present the results of the PMET rate obtained with the explicit permanent dipoles, which gives visually indistinguishable results from those obtained with only the transition dipole.

We further assume that the transition dipole moment $\boldsymbol{\mu}_{DA} = \langle D|\hat{\boldsymbol{\mu}}|A\rangle$ is always aligned with the polarization direction $\hat{\mathbf{e}}$ such that

$$\hat{\boldsymbol{\mu}} \cdot \hat{\mathbf{e}} = \boldsymbol{\mu}_{DA} \cdot \hat{\mathbf{e}}(|D\rangle\langle A| + |A\rangle\langle D|) \equiv \mu_{DA}(|D\rangle\langle A| + |A\rangle\langle D|), \quad (8)$$

where we have defined $\mu_{DA} \equiv \boldsymbol{\mu}_{DA} \cdot \hat{\mathbf{e}}$.

The light–matter interaction $\hat{H}_{int} = \boldsymbol{\chi} \cdot \hat{\boldsymbol{\mu}}(\hat{a}^\dagger + \hat{a}) + (\boldsymbol{\chi} \cdot \hat{\boldsymbol{\mu}})^2/\hbar\omega_c$ in Eq. (1) for the above model system is then given as

$$\hat{H}_{int} = \hbar g_c(|D\rangle\langle A| + |A\rangle\langle D|)(\hat{a}^\dagger + \hat{a}) + \frac{1}{2\epsilon_0 \mathcal{V}}(\hat{\boldsymbol{\mu}} \cdot \hat{\mathbf{e}})^2, \quad (9)$$

where the coupling strength $\hbar g_c \equiv \sqrt{\frac{\hbar\omega_c}{2\epsilon_0 \mathcal{V}}}\mu_{DA}$, and the second term in Eq. (9) is referred to as the dipole self-energy. For a two-state system without any permanent dipole moment, $(\hat{\boldsymbol{\mu}} \cdot \hat{\mathbf{e}})^2 = \mu_{DA}^2(|D\rangle\langle D| + |A\rangle\langle A|)$, which causes a constant energy shift for both electronic states, and hence, it is ignored for this special case.

The polariton Hamiltonian is defined as $\hat{H}_{pl} = \hat{H}_{PF} - \hat{P}_s^2/2M_s - \hat{H}_{sb}$, where the polariton states are the eigenstates of $\hat{H}_{pl}$ through the following eigenequation:

$$\hat{H}_{pl}|\Psi_i(R_s)\rangle = \mathcal{E}_i(R_s)|\Psi_i(R_s)\rangle, \quad (10)$$

where $\mathcal{E}_i(R_s)$ is the polariton eigenenergy. Note that the characters of the polariton states change[58] as a function of R_s. The above equation can be numerically solved by using the basis $\{|D, n\rangle, |A, m\rangle\}$.

Figure 1 illustrates quantizing the photon field through Fock states as well as through the ring polymer description. Figure 1(a) presents the quantum evolution of the light–matter hybrid system under the Fock state representation of the photon field. The nuclear wavepacket evolves among the photon-dressed electronic states $|D, n\rangle = |D\rangle \otimes |n\rangle$ (the donor electronic state with n photons inside the cavity) and $|A, m\rangle = |A\rangle \otimes |m\rangle$ (the acceptor electronic state with m photons inside the cavity), where $|n\rangle$ and $|m\rangle$ are the Fock states (eigenstates) of the vacuum photon field $\hat{H}_P = (\hat{a}^\dagger \hat{a} + \frac{1}{2})\hbar\omega_c$. While Fock states provide an exact quantum
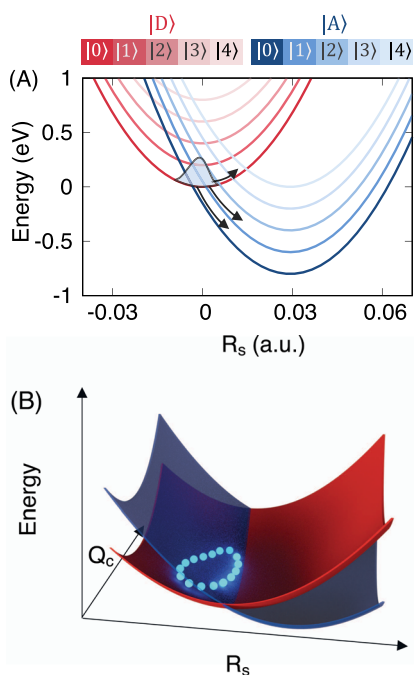
FIG. 1. Schematic illustrations of the polariton mediated electron transfer model. (a) The model system described with explicit Fock state quantization of the photon field coordinate Q_c, where $|D\rangle$ and $|A\rangle$ refer to the donor and acceptor electronic states and $|n\rangle \in \{|1\rangle, |2\rangle, \ldots\}$ represents the vacuum's Fock states. (b) Schematic illustration of the ring polymer quantization (cyan beads) of the photonic (and nuclear) DOFs. The cavity donor (red) and the acceptor (blue) diabatic surfaces are depicted as a function of the solvent coordinate R_s and the photonic coordinate Q_c.

mechanical description of the cavity mode and polariton quantum dynamics, a lot of them are required to achieve converged results for treating the light–matter interactions, especially when the coupling strength is in the strong and ultra-strong coupling regime.[21] In addition, the required number of Fock states will grow exponentially when multiple cavity modes are considered,[27] making this approach computationally expensive. For example, when considering a single molecule coupled to $\mathcal{M}$ cavity modes, each mode requires $\mathcal{K}$ Fock states, the size of the Hilbert space for the cavity modes then becomes $\mathcal{K}^{\mathcal{M}}$, and the numerical cost of propagating the time-dependent Schrodinger equation for these Fock states scales as $(\mathcal{K}^{\mathcal{M}})^2 = \mathcal{K}^{2\mathcal{M}}$.

Figure 1(b) schematically presents the quantum evolution of a light–matter hybrid system when using the ring polymer quantization. Here, the electronic DOFs are described with two diabatic states, $|D\rangle$ (red) and $|A\rangle$ (blue). The nuclei **R** and the photon field coordinate Q_c are quantized with the ring polymer representation. The ring polymer evolves on the 2-dimensional diabatic electronic potential energy surfaces and undergoes non-adiabatic transitions between $|D\rangle$ and $|A\rangle$. Compared to the exponential scaling of the Fock state quantization, the computational cost of quantizing the photon field with ring polymer scales linearly when considering

multiple radiation modes. With $\mathcal{N}$ beads for each mode, the computational cost for describing $\mathcal{M}$ modes is $\mathcal{N} \cdot \mathcal{M}$, which is more favorable than the scaling of the Fock state quantization approach $\mathcal{K}^{2\mathcal{M}}$ when considering a large number of cavity modes. Note that when using the same level of trajectory-based approaches to treat nuclear DOF, both descriptions of the photon field require a similar amount of trajectories to converge; thus, the pre-factors of both approaches are comparable.

B. Analytical rate theory

In this work, we use Fermi's Golden Rule (FGR) analytical rate expressions[8,62,63] as a benchmark for our numerical simulations. More specifically, we use Marcus rate theory to describe the ET rate of a molecule and use FGR[62] to describe the PMET rate in PMET. We also use the fluctuating ET theory to assess the classical limit (low frequency) of the cavity mode. We note that all of the analytical rate theories we used here correspond to the short-time limit of FGR[64,65] where the rate constant is insensitive to nuclear dynamics (solvent R_s and bath $\hat{H}_{sb}$). Details of the time-domain FGR rate and the short-time approximations are discussed in the supplementary material. The model parameter chosen for $\hat{H}_m$ in this study, on the other hand, ensures that the nuclear dynamics does not influence the rate. Recent developments of the accurate FGR expression through the linearized path-integral approach[66–68] have significantly expand the scope and applicability of the condensed phase ET[66–68] and non-equilibrium ET calculations,[69,70] going beyond the usual harmonic phonon approximations. We believe that these new advanced FGR approaches are also well suited for investigating PMET within the non-adiabatic limit. The NRPMD method, along the same line of the linearized path-integral FGR,[66–70] offers a general theoretical framework to simulate PMET reaction without any restrictions and the numerical capacity to treat the anharmonic bath environment[71,72] (in $\hat{H}_{sb}$) and strong electronic coupling and light–matter couplings that go beyond the capability of FGR.[58] In Sec. III, we provide further numerical tests for the cases when the FGR is no longer valid to describe PMET. We use the Fock state quantization of the photon field (and Ehrenfest approach for state-dependent dynamics) as a benchmark for direct NRPMD polariton quantum dynamics simulations.

(1) **Marcus theory for ET.** For the ET model system considered in this work, the equilibrium rate constant for the non-adiabatic electron transfer reaction between donor and acceptor states can be accurately described by Marcus theory (MT),[73]

$$k_{MT} = \frac{|V_{DA}|^2}{\hbar} \sqrt{\frac{\pi\beta}{\lambda}} \exp\left[-\beta \frac{(\Delta G + \lambda)^2}{4\lambda}\right], \qquad (11)$$

where ΔG is the ET driving force, λ is the reorganization energy, V_{DA} is the diabatic coupling between donor and acceptor states, and $\beta = 1/k_B T$, where k_B is the Boltzmann constant and T is the temperature of the system.

(2) **FGR for PMET.** For the molecule-cavity hybridized system, the polariton mediated electron transfer (PMET) occurs from a set of photon-dressed donor states $|D, n\rangle$ to a set of photon-dressed acceptor states $|A, m\rangle$. To explicitly calculate the rates

associated with each photon-dressed channel, we follow the previous theoretical work[8,62,63] and use Fermi's golden rule (also known as the Jortner theory[74–76] in ET) described as follows:

$$k_{FGR} = \sum_n \mathbb{P}_n \sum_m \frac{|F_{nm}|^2}{\hbar} \sqrt{\frac{\pi\beta}{\lambda}} \exp\left[-\beta \frac{(\Delta G_{nm} + \lambda)^2}{4\lambda}\right], \quad (12)$$

where $F_{nm} = \langle D, n|\hat{H}_{pl}|A, m\rangle = V_{DA}\delta_{nm} + \hbar g_c[\sqrt{m+1}\delta_{n,m+1} + \sqrt{m}\delta_{n,m-1}]$ is the effective coupling among photon-dressed states, $\hat{H}_{pl} = \hat{H}_{PF} - \hat{T}_s - \hat{H}_{sb}$ is the polariton Hamiltonian, $\hbar g_c$ is the effective light–matter coupling [see Eq. (9)], $\Delta G_{nm} = \Delta G + (m - n)\hbar\omega_c$ is the driving force between photon-dressed states, and $\mathbb{P}_n = \exp[-\beta n\hbar\omega_c]/\sum_m \exp[-\beta m\hbar\omega_c]$ is the thermal population of the corresponding cavity mode. Here, we treat n and m as a convergence parameter and use large enough Fock states to converge the rate. Note that the presence of zero-point energy (ZPE) of the radiation field is exactly canceled inside $\mathbb{P}_n$, hence not directly impacting the PMET rate. The quantized nature of the photon states, on the other hand, indeed significantly influences the PMET rate through F_{nm} and ΔG_{nm}. When treating the photonic DOF through quasi-classical descriptions (such as through the Wigner initial distributions), the zero-point energy leakage problem, on the other hand, could contaminate the electronic dynamics and lead to a less accurate PMET rate constant, as shown in our results.

When explicitly considering the presence of the permanent dipoles μ_{DD} and μ_{AA} associated with the diabatic electronic states $|D\rangle$ and $|A\rangle$, the PMET rate in Eq. (12) can be generalized as follows:[62]

$$k_{FGR} = \sum_n \mathbb{P}_n \sum_m \frac{|\tilde{F}_{nm}|^2}{\hbar} \sqrt{\frac{\pi\beta}{\lambda}} \exp\left[-\beta \frac{(\Delta G_{nm} + \lambda)^2}{4\lambda}\right], \quad (13)$$

where $\tilde{F}_{nm} = V_{DA}S_{nm} + \hbar g_c[\sqrt{n}S_{n-1,m} + \sqrt{n+1}S_{n+1,m}]$ is the effective coupling among photon-dressed states and $S_{nm} = \langle n|e^{-\frac{i}{\hbar}\hat{P}_c\sqrt{\frac{2}{\hbar\omega_c^3}}\chi\Delta\mu}|m\rangle$, where $\Delta\mu = \mu_{DD} - \mu_{AA}$. Here, we assume that all dipoles are aligned with $\hat{e}$ such that $\chi \cdot (\mu_{DD} - \mu_{AA}) = \chi(\mu_{DD} - \mu_{AA})$, where $\chi = \sqrt{\frac{\hbar\omega_c}{2\varepsilon_0 \mathcal{V}}}$. As one can clearly see that under the limit of a small $\Delta\mu$, the permanent dipole does not play a significant role in PMET. A detailed proof of Eq. (13) together with additional numerical results of the PMET rate with permanent dipoles is provided in the supplementary material.

(3) **Marcus theory with a fluctuating coupling.** We further view the cavity radiation mode as a Peierls coupling mode,[77–90] i.e., a fluctuating off-diagonal coupling term in the light–matter interaction Hamiltonian $\hat{H}_{int}$ [Eq. (9)], which can modulate the static electronic coupling (V_{DA}) between the donor and acceptor states. This, of course, is only valid when the photon frequency approaches the classical limit $\hbar\omega_c \ll k_B T$.

This Peierls fluctuated electronic coupling for the model in Eq. (9) is expressed as

$$V_{DA}(Q_c) = \langle D|\hat{H}_m + \hat{H}_{int}|A\rangle = V_{DA} + \sqrt{2\omega_c}g_c Q_c. \quad (14)$$

The variance σ_{DA}^2 characterizes the magnitude of the fluctuation around the static value of $\langle V_{DA}(Q_c)\rangle = V_{DA}$, which is

$$\sigma_{DA}^2 = \langle V_{DA}^2(Q_c)\rangle - \langle V_{DA}(Q_c)\rangle^2 = 2\omega_c g_c^2\langle Q_c^2\rangle, \quad (15)$$

where $\langle Q_c^2\rangle = 1/\beta\omega_c^2$ based on the classical distribution of the photon mode Q_c. With the presence of Peierls coupling, the V_{DA} term in the MT [Eq. (11)] needs to be modified as $V_{DA}(Q_c)$ [Eq. (14)], and the Marcus theory with the Peierls coupling can be expressed as[81,85]

$$k_{MT}^P = \frac{\langle V_{DA}^2(Q_c)\rangle}{\hbar} \sqrt{\frac{\pi\beta}{\lambda}} \exp\left[-\beta \frac{(\Delta G + \lambda)^2}{4\lambda}\right], \quad (16)$$

where the mean square coupling $\langle V_{DA}^2(Q_c)\rangle = V_{DA}^2 + \sigma_{DA}^2$ includes both static contribution and the fluctuations induced by the photon field. Depending on the relative magnitude of V_{DA}^2 and σ_{DA}^2, the ET rate is controlled by either the averaged electronic coupling square or the variance squared term.[82] Note that when deriving Eq. (16), the donor–acceptor energy gap fluctuations are assumed to be uncorrelated to the fluctuations of the off-diagonal coupling as these two types of fluctuations are originated from different sets of nuclear modes.[81] Our PMET model studied here indeed satisfies this uncorrelated assumption. The off-diagonal fluctuations in our PMET model are caused by the photonic DOF Q_c, and the diagonal fluctuations are caused from the solvent coordinate R_s and bath coordinates $\{R_k\}$.

C. NRPMD simulations of PMET

We aim to compute the reduced density matrix of the light–matter hybrid system

$$\rho_{jj}(t) = \mathrm{Tr}_e \mathrm{Tr}_R \mathrm{Tr}_{Q_c}[\hat{\rho}_0 e^{i\hat{H}t/\hbar}\hat{\mathcal{P}}_j e^{-i\hat{H}t/\hbar}], \quad (17)$$

where $\rho_{jj}(t)$ is the time-dependent population of the diabatic state $|j\rangle \in \{|D\rangle, |A\rangle\}$, $\hat{\mathcal{P}}_j = |j\rangle\langle j|$ is the associated projection operator, and Tr_R represents the trace over all nuclear DOF (including solvent R_s and the bath $\{R_k\}$), Tr_{Q_c} represents the trace over the photonic DOF, and Tr_e represents the trace over the electronic DOF in the $\{|D\rangle, |A\rangle\}$ subspace.

For a cavity-free charge transfer reaction, the initial condition is sampled based upon the quantum canonical distribution of the Hamiltonian,[64,91,92] $\hat{\mathcal{P}}\hat{H}_m\hat{\mathcal{P}}$, where the projection operator $\hat{\mathcal{P}} = |D\rangle\langle D|$ confines $\hat{H}_m$ inside the $|D\rangle$ subspace. Similarly, the initial density operator of the reactant state for the light–matter

hybrid system should correspond to the quantum canonical density associated with the hybrid system confined in the donor electronic subspace as $\hat{\mathcal{P}}\hat{H}_{PF}\hat{\mathcal{P}}$. When only considering the transition dipole in the light–matter interactions, $\langle D|\hat{H}_{int}|D\rangle = \frac{1}{2\epsilon_0 \mathcal{V}}\mu_{DA}^2$ with $\hat{H}_{int}$ in Eq. (9). Note that this term [coming from the dipole self-energy (DSE) term] has a constant value (due to our assumption that μ_{DA} is a constant) and is not a function of R_s or Q_c. Thus, the initial canonical density associated with $\hat{\mathcal{P}}\hat{H}_{PF}\hat{\mathcal{P}}$ is $\hat{\rho}_0 = |D\rangle\langle D| \otimes \hat{\rho}_R \otimes \hat{\rho}_{Q_c}$, which is a direct product of the initial donor electronic state $|D\rangle$ with the initial nuclear density operator $\hat{\rho}_R = e^{-\beta \hat{H}_R}/\mathcal{Z}_R$, where $\hat{H}_R = \frac{1}{2M_s}\hat{P}_s^2 + \frac{1}{2}M_s\omega_s^2(\hat{R}_s - R_D^0)^2 + \hat{H}_{sb}$ and the initial distribution of the photon mode $\hat{\rho}_{Q_c} = e^{-\beta(\hat{a}^\dagger \hat{a} + \frac{1}{2})\hbar\omega_c}/\mathcal{Z}_{Q_c}$. Furthermore, $\mathcal{Z}_R$ and $\mathcal{Z}_{Q_c}$ are the corresponding partition functions for the nuclear and photonic DOFs. Choosing the initial electronic state as $|D\rangle$, the distribution of the solvent coordinate R_s is centered around R_D^0 and the distribution of the photonic coordinate is centered around $Q_c = 0$.

On the other hand, for a model system where the transition dipole is not a constant, i.e., $\hat{\mu} \cdot \hat{e} = \mu_{DA}(R_s)(|D\rangle\langle A| + |A\rangle\langle D|)$, the light–matter interaction in $\hat{\mathcal{P}}\hat{H}_{PF}\hat{\mathcal{P}}$ is no longer a constant, but rather $\langle D|\hat{H}_{int}|D\rangle = \frac{1}{2\epsilon_0 \mathcal{V}}\mu_{DA}(R_s)^2$. This part will influence the initial distribution of R_s. Furthermore, when explicitly considering the constant permanent dipole μ_{DD} (as well as the constant transition dipole μ_{DA}), the light–matter interaction in Eq. (9) becomes $\langle D|\hat{H}_{int}|D\rangle = \sqrt{\frac{2\omega_c}{\hbar}}\chi\mu_{DD} \cdot \hat{Q}_c + \frac{1}{2\epsilon_0 \mathcal{V}}(\mu_{DD}^2 + \mu_{DA}^2)$, and the photonic coordinate will be shifted accordingly for sampling the canonical distribution associated with $\hat{\mathcal{P}}\hat{H}_{PF}\hat{\mathcal{P}}$. The details for this case are provided in the supplementary material.

We use the NRPMD Hamiltonian in Eq. (2) to simulate the molecule-cavity hybrid system and compute the time-dependent reduced density matrix $\rho_{jj}(t)$ defined in Eq. (17) through the following population expression:[31,36]

$$\rho_{jj}(t) \approx \int d\tau \mathcal{P}^0(\{\mathbf{q}_\alpha, \mathbf{p}_\alpha\})\rho_{rp}(\{\mathbf{X}_\alpha, \mathbf{\Pi}_\alpha\}) \cdot \bar{\mathcal{P}}_j(t), \quad (18)$$

where $\mathbf{X} \equiv \{\mathbf{R}, Q_c\}$, $\mathbf{\Pi} \equiv \{\mathbf{P}, P_c\}$, and $d\tau \equiv \int d\{\mathbf{X}_\alpha\}d\{\mathbf{\Pi}_\alpha\}d\{\mathbf{q}_\alpha\}d\{\mathbf{p}_\alpha\}$ with a shorthand notation $d\{\boldsymbol{\xi}_\alpha\} = \prod_{\alpha=1}^{\mathcal{N}} d\boldsymbol{\xi}_\alpha$. In addition, $\mathcal{P}^0(\{\mathbf{q}_\alpha, \mathbf{p}_\alpha\})$ represents the distribution of the initial electronic variables and $\rho_{rp}(\{\mathbf{X}_\alpha, \mathbf{\Pi}_\alpha\})$ represents the initial ring polymer distribution of both the nuclear and photonic DOFs that corresponds to $\hat{\rho}_R \otimes \hat{\rho}_{Q_c}$. Finally, $\bar{\mathcal{P}}_j = \frac{1}{\mathcal{N}}\sum_\alpha \mathcal{P}_j(\alpha) = \frac{1}{\mathcal{N}}\sum_{\alpha=1}^{\mathcal{N}} \frac{1}{2}([\mathbf{q}_\alpha]_j^2 + [\mathbf{p}_\alpha]_j^2 - 1)$ is the electronic state estimator that has shown[31,33] to provide accurate results for non-adiabatic dynamics. Other choices of the initial conditions for the mapping variables, such as the symmetric quasi-classical window approaches,[93,94] have shown to further improve the population dynamics, and we plan to explore these choices in the future.

In this work, because the solvent R_s and the bath coordinates $\{R_k\}$ have low vibrational frequencies (hence exhibiting quasi-classical behavior), we use $\mathcal{N} = 1$ bead for these DOFs. Thus, the initial distribution of the solvent and the bath DOFs corresponds to a pure classical distribution $\rho_R = e^{-\beta H_R}/\mathcal{Z}_R$, where $H_R = \frac{1}{2M_s}P_s^2 + \frac{1}{2}M_s\omega_s^2(R_s - R_D^0)^2 + H_{sb}$. For the photonic ring polymer, we treat the number of beads $\mathcal{N}$ as a convergence parameter such that the initial

distribution $\rho_{rp}([Q_c]_\alpha, [P_c]_\alpha)$ is converged.[31,36] The same number of beads is used for the mapping variables,[31] with the initial density[31,36] $\mathcal{P}^0(\{\mathbf{q}_\alpha, \mathbf{p}_\alpha\}) = \prod_{\alpha=1}^{\mathcal{N}}\prod_{j=1}^{\mathcal{F}} \delta(\mathcal{P}_j(\alpha) - \rho_{jj}(0))$ that is properly constrained to represent the initially occupied state $|D\rangle$ through $\mathcal{P}_j(\alpha) = \frac{1}{2}([\mathbf{q}_\alpha]_j^2 + [\mathbf{p}_\alpha]_j^2 - 1) = \delta_{Dj}$. The details of the sampling procedure are provided in the supplementary material. All DOFs are then propagated using the Hamilton's equation of motion according to the Hamiltonian in Eq. (2). For all of the results presented in this work, a total of 10^4 trajectories are used to ensure the tight convergence of population [based on Eq. (18)], although 10^3 trajectories already present the basic trend of the dynamics.

With the converged population dynamics, we use a rate fitting scheme[91,92] (details are provided in the supplementary material) to obtain the PMET rate of the reaction. In general, the charge transfer rate constant can be obtained by using the flux–side correlation function formalism[95] $k = Q_r^{-1} \lim_{t\to t_p} \text{Tr}_\mathbf{R}[\hat{\rho}\hat{F}e^{i\hat{H}t/\hbar}\hat{h}e^{-i\hat{H}t/\hbar}]$, where the side operator $\hat{h} = \sum_n |A, n\rangle\langle A, n|$ represents the dividing surface distinguishing reactant and product (where n is the number of photons in the cavity), $\hat{F} = i/\hbar[\hat{H}, \hat{h}]$ is the flux operator, t_p is the plateau time of the correlation function, $\hat{\rho} = e^{-\beta\hat{H}}$ is the thermal density operator, and $Q_r = \text{Tr}[\hat{\rho}\hat{h}]$ is the reactant partition function. It requires, however, additional theoretical development to use NRPMD for computing the Kubo-transformed version of this correlation function. Hence, we choose to compute the population dynamics with NRPMD and use the well-defined fitting procedure to obtain the rate.[91,92]

D. Additional theoretical approaches

To further assess the accuracy of the ring polymer quantization of the cavity photon field, we compare it with the following theoretical descriptions of the cavity photon field, where the state-dependent non-adiabatic dynamics are propagated with the multi-trajectory Ehrenfest approach.[25]

(i) **Classical:** using a classical distribution of the photon field and Ehrenfest dynamics to propagate the non-adiabatic dynamics.

(ii) **Wigner:** using the Wigner initial distribution of the photon field[25–27] and Ehrenfest dynamics to propagate the non-adiabatic dynamics.

(iii) **Fock states:** using Fock states to represent the polariton Hamiltonian $\hat{H}_{pl} = \hat{H}_{PF} - \hat{T}_s - \hat{H}_{sb}$ and then propagate the quantum dynamics in the diabatic-Fock basis $\{|D, n\rangle, |A, m\rangle\}$.

For each of the above approaches, a total of 10^4 trajectories are used to make sure both convergence and a consistent comparison with the NRPMD calculations. The details of all the above approaches are provided in the supplementary material.

E. Model parameters

In this work, we consider the following four model parameters for the molecular Hamiltonian and light–matter interactions, presented in Table I.

TABLE I. Model parameters used in the light–matter interaction Hamiltonian.

Model	V_{DA} (meV)	$\hbar g_c$ (meV)	$\hbar\omega_c$ (meV)
I	5	3	10
II	5	5	200
III	30	5	200
IV	5	20	200

Models I and II have weak electronic coupling parameters ($\beta V_{DA} \ll 1$). For model I, the parameters are chosen for the theoretical purpose to achieve a classical limit of the cavity field. Parameters for model II are chosen according to the recent theoretical work by Semenov and Nitzan,[62] which are chosen by closely connecting to the available polariton experimental setup. For both models I and II, $\hbar g_c$ and V_{DA} are chosen to be small [such that $|F_{nm}| \ll k_B T$ in Eq. (12)], and Fermi's golden rule (FGR) is valid, which can be used as a benchmark for our direct dynamics simulation.

Moreover, models III and IV are chosen such that $|F_{nm}| \sim k_B T$ (where $F_{nm} = \langle D, n|\hat{H}_{pl}|A, m\rangle = V_{DA}\delta_{nm} + \hbar g_c[\sqrt{m+1}\delta_{n,m+1} + \sqrt{m}\delta_{n,m-1}]$) in Eq. (12); thus, the FGR description (which requires $|F_{nm}| \ll k_B T$) of the PMET rate constant breaks down. The photon frequency for both models is chosen to be $\hbar\omega_c = 200$ meV, with two possible choices of electronic coupling and light–matter coupling; for model III, $V_{DA} = 30$ meV and $\hbar g_c = 5$ meV, and for model IV, $V_{DA} = 5$ meV and $\hbar g_c = 20$ meV. For case III, the FGR breaks down because of the large V_{DA}, whereas for case IV, FGR is no longer valid due to the strong light–matter interactions $\hbar g_c$.

III. RESULTS AND DISCUSSIONS

Figure 2 presents the PMET rate of the molecule-cavity hybrid system over a range of driving force ($-\Delta G$), with both model I in Fig. 2(a) and model II in Fig. 2(b). The NRPMD approach (red dots) with a total of $\mathcal{N} = 4$ and $\mathcal{N} = 8$ beads are used to generate converged results for model I [panel (a)] and model II [panel (b)], respectively. We emphasize that for model I, only $\mathcal{N} = 1$ bead will be sufficient enough for generating converged results because of the low frequency photon mode ($\hbar\omega_c = 10$ meV) used there. The PMET rate constants obtained from the NRPMD simulations (red dots) are compared against the FGR rate when the molecule is explicitly coupled to the cavity (black solid lines) and when the molecule is decoupled from the cavity (blue dashed line). For the model used here, the solvent DOF R_s has a low vibrational frequency that does not exhibit any nuclear quantum effects at $T = 300$ K. As a result, we can see one single turnover of the ET rate as $-\Delta G$ increases when the molecule is decoupled from the cavity (blue dashed lines in both panels) where the charge transfer occurs via $|D\rangle \rightarrow |A\rangle$, and the rate peaks at $-\Delta G = \lambda$, known as the Marcus turnover.[73,96]

With the presence of the cavity, the charge transfer occurs from the photon-dressed donor states $|D, n\rangle$ to the photon-dressed acceptor states $|A, m\rangle$. When the cavity has a low photon frequency $\hbar\omega_c = 10$ meV [Fig. 2(a)] such that $\hbar\omega_c \ll k_B T$, one needs to explicitly
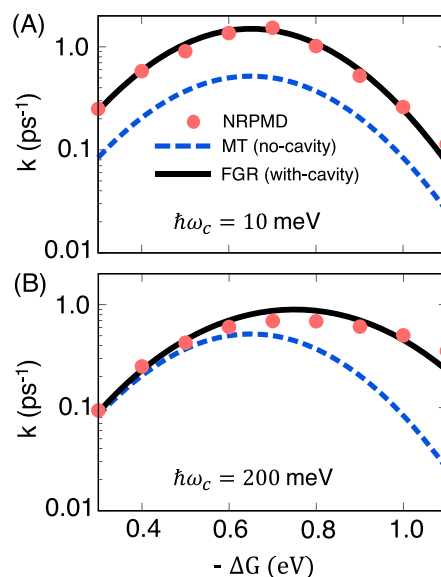

FIG. 2. PMET rate constants of a molecule-cavity hybrid system over a range of $-\Delta G$ with (a) $\hbar\omega_c = 10$ meV and (b) $\hbar\omega_c = 200$ meV. The rate constants are obtained from the NRPMD simulations (red dots), and the PMET rate (black solid lines) is obtained from FGR [Eq. (12)]. Marcus theory [Eq. (11)] for the cavity-free ET rate constant (blue dashed lines) is presented for comparison.

consider reactive channels for those n, $m \geq 1$. This is because the excited photon-dressed donor states, $|D, 1\rangle$, $|D, 2\rangle$, ..., etc., are thermally accessible, and as a result, the predominant reactive channel is not only $|D, 0\rangle \rightarrow |A, 0\rangle$, but there is also a significant contribution from other high-lying photon-dressed states. As a result, the PMET rate [described by FGR in Eq. (13)] is significantly enhanced throughout all ranges of driving forces compared to the cavity-free case [described by the MT rate in Eq. (11)]. Quantizing the radiation mode with the ring polymer description (through the NRPMD approach) provides quantitatively accurate results compared to the FGR analytical rate theory for PMET.

Figure 2(b) presents the PMET rate for the light–matter hybrid system with a high photonic frequency $\hbar\omega_c = 200$ meV such that $\hbar\omega_c \gg k_B T$. In this case, the photon frequency is high enough such that under the room temperature, only $|D, 0\rangle$ has an appreciable amount of thermal population. At a small driving force $-\Delta G < \lambda$, the predominant reactive channel is $|D, 0\rangle \rightarrow |A, 0\rangle$, and the channel $|D, 0\rangle \rightarrow |A, 1\rangle$ is less favorable due to the large energy difference between these two photon-dressed states. Hence, the PMET rate constant (from FGR) in this parameter regime is close to the ET rate of the molecule (through the $|D, 0\rangle \rightarrow |A, 0\rangle$ reactive channel) without the coupling with the cavity. At a larger driving force, $-\Delta G \geq \lambda$ (Marcus inverted regime), the photon-dressed acceptor state $|A, 1\rangle$ is energetically closer to the $|D, 0\rangle$ state, and hence, the rate constant is higher than the Marcus ET rate in the inverted regime due to this additional channel.

Thus, the high-frequency radiation mode plays a similar role as those high-frequency vibrational modes do.[75] In this sense, the PMET process is akin to the proton-coupled electron transfer

(PCET) reaction, where the presence of quantized vibrational levels of the transferring proton mediates the effective vibronic couplings as well as the effective state-to-state driving force.[97,98] In PMET, the presence of quantized photonic states of the cavity radiation mode mediates the effective vibronic couplings and the effective state-to-state driving force. Again, the ring polymer description of the photon field provides a quantitatively correct answer compared to the FGR results, similar to the success of the ring polymer quantization of the proton,[37,54] which provides an accurate PCET rate constant. As a side note, it is also interesting to observe the success of the NRPMD approach to correctly predict the Marcus turnover as well as the rate enhancement in the inverted regime when the electronic subsystem is coupled to the quantum (photonic) mode. This accurate numerical performance of NRPMD goes beyond the mean-field RPMD approach,[99] which shows a less accurate rate constant in the inverted regime.[99]

Figure 3 presents the detailed comparisons of the PMET rate constants and polariton quantum dynamics obtained from various theoretical treatments of the photon field, including the ring polymer quantization (red dots), Fock state quantization (cyan open circles), Wigner distribution (dashed orange line), and classical distribution (dashed green line) of the radiation mode. For the Fock state description, we have used a total of five Fock states for model II (although two Fock states already generate visually indistinguishable results), whereas 15 Fock states are required for model I (results not shown here).
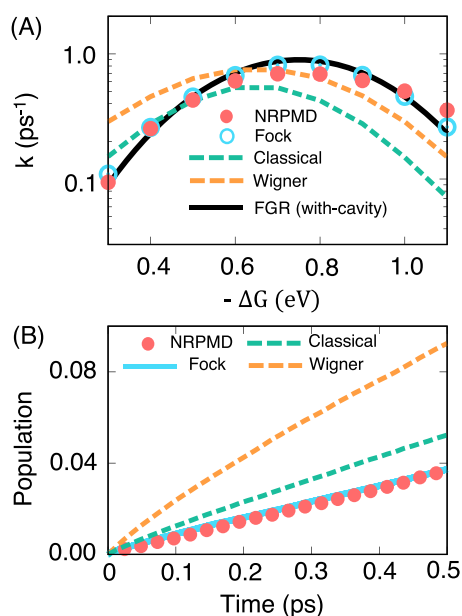
FIG. 3. (a) The PMET rate constant of model system II with $\hbar\omega_c$ = 200 meV, obtained from different photon quantization approaches, including the ring polymer quantization with NRPMD (red filled circles), the Fock state quantization (cyan open circles), classical description (green dashed line), and Wigner quantization (orange dashed line) of the photon mode. (b) The corresponding acceptor state population dynamics $\rho_{AA}(t)$.
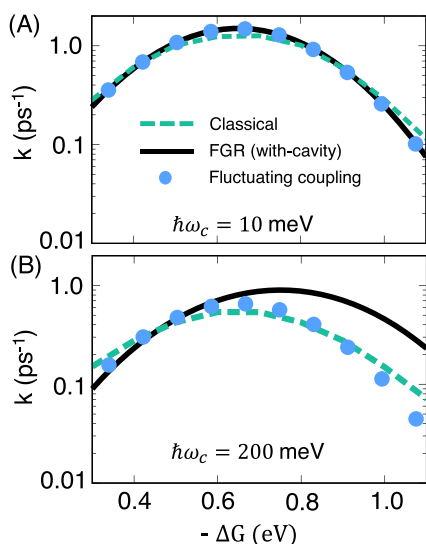
Figure 3(a) presents the PMET rate of the model system with $\hbar\omega_c$ = 200 meV [same model in Fig. 2(b)] obtained from different theoretical approaches, with FGR rate theory (black solid line) as a benchmark of the quantum result. It can be clearly seen that treating the radiation mode with a classical initial distribution (green dashed line) does not account for the quantum effects associated with the high-frequency photon modes and thus fails to predict the accurate PMET rate constant throughout the entire range of driving force. Furthermore, in contrast to the previous results of cavity QED,[25–28] treating the photon mode with the initial Wigner distribution (orange dashed line) also fails to provide the quantitative results of the rate constants. The breakdown of the classical Wigner model is likely due to the fact that the classical equation of motion for the photon field in this calculation[29,31,100] leads to the incorrect flow of the photonic energy (from the Wigner distribution) to the electronic subsystem. Finally, we also quantize the photon field through the Fock state description (cyan open circles), and this description provides the most accurate results of the PMET rate constant (compared to FGR) due to the explicit quantum mechanical description of the radiation mode as well as all reactive channels.

While quantizing the photon field with Fock states provides accurate results, it is limited in terms of how many radiation modes can be explicitly treated. The ring polymer quantization, on the other hand, provides the same level of accuracy while significantly reducing the computational costs by using the extended classical phase space description. Note that both the Fock state quantization and the NRPMD simulation presented in this paper are trajectory-based approaches (multi-trajectory Ehrenfest and NRPMD approach, respectively), and both require 10^4 trajectories to achieve numerical convergence. Through a similar amount of trajectories, the Fock state quantization with Ehrenfest dynamics requires initial sampling for the nuclear DOFs, whereas the NRPMD approach samples both the initial nuclear configurations and the ring polymer configurations for the photonic DOF. This provides a consistent framework to meaningfully compare the numerical cost of the ring polymer and the Fock state quantization of the cavity modes, specifically for model parameter II, which requires $\mathcal{K}$ = 5 Fock states or $\mathcal{N}$ = 8 beads to converge the polariton quantum dynamics. Considering $\mathcal{M}$ = 2 cavity modes, the corresponding computational costs for the Fock state or the ring polymer description are $\mathcal{K}^{2\mathcal{M}} = 5^4$ = 625 and $\mathcal{N} \cdot \mathcal{M} = 10 \times 2$ = 20, respectively. Our numerical test (see details in the supplementary material) confirms this scaling and the advantage of the ring polymer quantization. In fact, even considering just one cavity mode, the numerical advantage of using the ring polymer quantization ($\mathcal{N} \cdot \mathcal{M} = 10 \times 1 = 10$) is already shown compared to the Fock state quantization ($\mathcal{K}^{2\mathcal{M}} = 5^2 \approx 25$).

Figure 3(b) presents the population dynamics of the acceptor state $\rho_{AA}(t)$ for the same molecule-cavity system presented in Fig. 3(a), with a particular driving force $-\Delta G$ = 300 meV. This figure further demonstrates the accuracy of the ring polymer quantization compared to other approaches, through the real-time population dynamics (and not only through the rate constant). We can clearly see that NRPMD (red dots) provides nearly identical population dynamics compared to the Fock state description of the photon field (cyan solid line), which, in principle, provides the most accurate polariton quantum dynamics [as shown in the rate constant in panel

(a)]. On the other hand, the Wigner quantization (orange dashed line) and the classical description (green dashed line) of the photon field fail to provide quantitatively accurate population dynamics. To confirm the failure of the Wigner description of the photon field, we further tested (see the results in the supplementary material) the $\mathcal{N} = 1$ bead case of the NRPMD approach, with either a Wigner or a classical initial distribution of the photonic DOF. Both simulations provide less accurate PMET dynamics (see the supplementary material), confirming that the numerical improvement we observed in Fig. 3 is directly associated with the ring polymer description of the photon field and not because of the MMST mapping representation in the NRPMD (which potentially brings improvement compared to the Ehrenfest approach).

Figure 4 compares the PMET results obtained from the Marcus theory with a fluctuating coupling (blue dots) in Eq. (16), the FGR rate (solid black line) in Eq. (12), as well as the classical treatment of the photon field (green dashed line). In Fig. 4(a), the model system has the same parameters as the one used in Fig. 2(a). At a low photonic frequency, the classical description of the radiation mode provides an accurate result because the quantum distribution of the photonic DOF is nearly identical with the classical distribution. Furthermore, the Marcus theory with a fluctuating coupling provides a quantitative agreement with the FGR rate. In this case, the photon mode can be viewed as a fluctuating Peierls-type of coupling (off-diagonal coupling in the $\{|D\rangle, |A\rangle\}$ subspace). The cavity mode fluctuates the value of the electronic coupling [see Eq. (15)] and significantly contributes to the rate [see Eq. (16)]. Under this low frequency regime, the cavity assisted charge transfer mechanism can be purely viewed as the fluctuation of the radiation mode that enhances the ele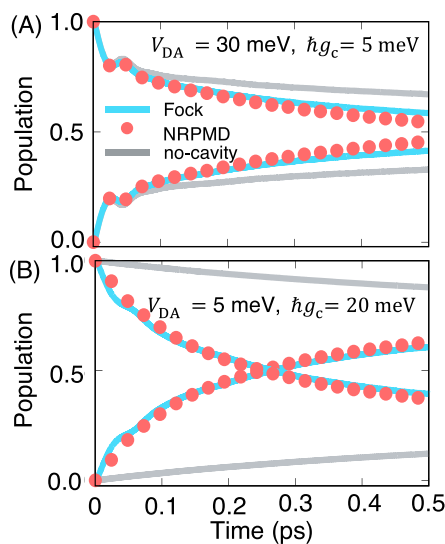ctronic coupling term. Similar effects have been well understood in charge transfer reactions in protein[81,82,85,87,90] as well as in singlet fission.[101–103] Our theoretical results imply that for the PMET reaction in the vibrational strong coupling regime (where the photon frequency is close to the vibrational frequency), the cavity mode acts like a fluctuating coupling term that can further enhance the ET rate.

Figure 4(b) presents the same comparison of the model system with a high cavity frequency [same parameters used in Fig. 2(b)]. Due to the high photonic frequency $\hbar\omega_c$, the classical description of photonic DOF is no longer capable of accurately capturing the quantum effect, especially the rate enhancement in the Marcus inverted regime. Furthermore, the Marcus theory with a fluctuating coupling deviates from the quantum FGR results but agrees with the classical description of the radiation mode since both of them use the classical treatment of the radiation mode. On the other hand, both the state-resolved FGR rate and the ring polymer quantization of the radiation field [Fig. 2(b)] provide accurate PMET rate constants under the high-frequency limit of the cavity mode.

Finally, Fig. 5 presents the population dynamics of models III [panel (a)] and IV [panel (b)] with a driving force of $-\Delta G = 0.8$ eV. Both model parameters are beyond the FGR regime, which requires $|F_{nm}| \ll k_B T$ in Eq. (12). The Fock state description (with $\mathcal{K} = 5$ Fock states) of the photon field (cyan) is used as a benchmark for the population dynamics. The populations of photon-dressed states $\{|D, n\rangle, |A, m\rangle\}$ are provided in the supplementary material. The ring polymer description of the photon field (red dots) with $\mathcal{N} = 16$ beads provides the converged results of the population dynamics, which has an excellent agreement with the Fock state description.

FIG. 4. PMET rate constants for (a) model I and (b) model II over a range of driving force ($-\Delta G$). The rates are obtained with the classical description of the photon mode (green dashed line), FGR rate in Eq. (12) (black solid line), and fluctuation mediated rate theory in Eq. (16) (blue dots).

FIG. 5. (a) The population dynamics [$\rho_{DD}(t)$ and $\rho_{AA}(t)$] for model III with $V_{DA} = 30$ meV and $\hbar g_c = 5$ meV. (b) The population dynamics for model IV with $V_{DA} = 5$ meV and $\hbar g_c = 20$ meV. The photon frequencies for both cases are $\hbar\omega_c = 200$ meV. The populations are obtained from the NRPMD simulations (red dots) and Fock state quantization (cyan solid line). The gray solid lines correspond to the population dynamics of the cavity-free case, obtained from the Ehrenfest dynamics governed by $\hat{H}_m$.

Similar to the results presented in Fig. 3(b), the Wigner or classical treatment of the cavity photon field provides less accurate results (which are provided in the supplementary material), even at a short time. The cavity-free dynamics (gray) is also presented for comparison. Figure 5(a) presents a case where the electronic coupling is large and beyond the FGR limit ($\beta V_{DA} > 1$) such that the population dynamics is no longer following a single exponential decay (described by a rate constant). Adding additional light–matter coupling further enhances the PMET process. Figure 5(b) presents a case where the electronic coupling is weak $\beta V_{DA} \ll 1$, and light–matter coupling is strong such that $F_{nm} \sim k_B T$. In fact, $g_c/\omega_c = 0.1$, which means the light–matter interactions start to enter into the ultra-strong coupling regime.[59,104] In this case, the large light–matter interaction significantly changes the population dynamics of the donor and acceptor compared to the cavity-free case (gray curves) and makes them non-exponential. For both cases, beyond the simple FGR limit, the ring polymer quantization provides an accurate description of the electronic dynamics influenced by the cavity.

Before we end this section, we want to comment on the potential limitations of using the NRPMD approach to simulate PMET dynamics. First, using the ring polymer extended phase space description for the cavity mode, one does not have an explicit access to the information related to Fock states or the polariton states $|\Psi_i(R_s)\rangle$ [defined in Eq. (10)]. Thus, we do not directly have the polariton population or coherence. Second, the success of any RPMD-based approach relies on the separation of the time-scale between the high-frequency vibrations of the ring polymer and the dynamics of physical interest.[44] The high-frequency ring polymer oscillations could potentially contaminate the real-time dynamics of the photonic DOF, which, in turn, influence the electronic quantum dynamics. We will investigate this issue in the future based on the previous work that has been shown to address this issue.[31]

IV. CONCLUSION

In this paper, to the best of our knowledge, we present the first numerical example of using the ring polymer representation[40,41,44] to quantize the cavity photon field in polariton chemistry. Using the recently developed non-adiabatic ring polymer molecular dynamics approach,[31,33,38] we investigate a charge transfer model coupled to an optical cavity.[8,58,62] Our numerical results suggest that the ring polymer quantization of the photon field provides accurate polariton mediated charge transfer rate constants and dynamics over a broad range of electronic driving force compared to Fermi's golden rule.[62] For the system beyond the FGR regime, the ring polymer quantization also gives accurate dynamics compared to the Fock state description of the cavity mode.

Our investigations provide further mechanistic insights into the polariton mediated electron transfer (PMET) reaction.[58,62] With a high photon frequency ($\hbar\omega_c > k_B T$), the cavity radiation mode acts like a quantized vibrational DOF, and PMET is analogous to proton-coupled electron transfer reactions.[97,98] With a low photon frequency ($\hbar\omega_c < k_B T$), the cavity mode plays a role in the classical fluctuating Peierls-type coupling, and PMET is analogous to ET reactions in a fluctuating environment such as protein.[81,82,85,87,90]

Compared to the Fock state description of the photon field, the ring polymer quantization provides the same level of accuracy and yet offers a computationally convenient framework to describe the polariton quantum effects through the extended phase space description. In contrast to the unfavorable scaling of Fock states, the extended phase space (ring polymer) description can easily treat multiple quantized modes inside the cavity and scales linearly with these photonic DOFs. Compared to the quasi-classical descriptions (such as the classical Wigner model) that cause zero-point energy (ZPE) leakage problems,[29] which contaminate the electronic dynamics,[31] the ring polymer description alleviates the ZPE leaking problem, thus reliably providing longer time electronic population dynamics.[31] These encouraging numerical results open up new possibilities for using NRPMD to accurately and efficiently simulate polaritonic chemistry with many molecules[8,19,63] coupled to many quantized radiation modes inside an optical cavity,[27] providing a set of general and powerful theoretical tools and frameworks for the emerging polariton chemistry community. We also note that the present approach can be extended to include cavity losses, which include the coupling between the cavity modes to a set of dissipative far-field modes.[105]

We envision that recently developed state-dependent RPMD approaches[33,35–38,55,106–108] should be well-suited for the investigation of polariton chemistry[27] and atomic cavity QED[25,26] when multiple photonic modes play a crucial role in polariton quantum dynamics.[27] In fact, because $\{\hat{P}_c, \hat{Q}_c\}$ in $\hat{H}_{PF}$ [Eq. (1)] can be viewed as an effective "nuclear" DOF that exhibits quantum effects, we conjecture that any approach in theoretical chemistry that can accurately treat nuclear quantization[42,44,109–112] will have a chance to be applicable to investigate polariton chemistry when explicit quantization of the cavity radiation mode is necessary. This "isomorphism" between the nuclear vibrations and cavity photonic modes[23–26,28] could also provide further insights into understanding new reactivities[113] in polariton chemistry. At the same time, this "isomorphism" allows one to transfer knowledge (methods or insights) from one field (physical and theoretical chemistry) to another field (atomic and molecular polariton physics) and facilitate the merger of both.

SUPPLEMENTARY MATERIAL

See the supplementary material for the details of the bath discretization and model parameters, non-adiabatic RPMD quantum dynamics, initial sampling procedure and details of the numerical simulations of NRPMD, details of other theoretical treatments of the photon field, fitting scheme for obtaining the rate constant, additional numerical results, and permanent dipole moment in PMET dynamics.

ACKNOWLEDGMENTS

APPENDIX: DERIVATION OF THE PAULI–FIERZ QED HAMILTONIAN

We provide a brief derivation of the Pauli–Fierz QED Hamiltonian. We begin by defining the matter Hamiltonian and the corresponding total dipole operator as follows:

$$\hat{H}_\mathrm{m} = \hat{\mathbf{T}} + \hat{V}(\hat{\mathbf{x}}) = \sum_j \frac{1}{2M_j} \hat{\mathbf{P}}_j^2 + \hat{V}(\hat{\mathbf{x}}), \quad \hat{\boldsymbol{\mu}} = \sum_j z_j \hat{\mathbf{x}}_j, \quad \text{(A1)}$$

where j is the index of the jth charged particle (including all electrons and nuclei), with the corresponding mass M_j and charge z_j. In addition, $\hat{\mathbf{x}} \equiv \{\hat{\mathbf{x}}_j\} = \{\hat{\mathbf{R}}, \hat{\mathbf{r}}\}$ with $\hat{\mathbf{R}}$ and $\hat{\mathbf{r}}$ representing the nuclear and electronic coordinates, respectively, and $\hat{\mathbf{P}} \equiv \{\hat{\mathbf{P}}_\mathbf{R}, \hat{\mathbf{P}}_\mathbf{r}\} \equiv \{\hat{\mathbf{P}}_j\}$ is the *mechanical* momentum operator as well as the canonical momentum operator such that $\hat{\mathbf{P}}_j = -i\hbar\nabla_j$. Furthermore, $\hat{\mathbf{T}} = \hat{\mathbf{T}}_\mathbf{R} + \hat{\mathbf{T}}_\mathbf{r}$ is the kinetic energy operator, where $\hat{\mathbf{T}}_\mathbf{R}$ and $\hat{\mathbf{T}}_\mathbf{r}$ represent the kinetic energy operator for nuclei and for electrons, respectively, and $\hat{V}(\hat{\mathbf{x}})$ is the potential operator that describes the Coulombic interactions among electrons and nuclei.

The cavity photon field Hamiltonian under the single-mode assumption is expressed as

$$\hat{H}_\mathrm{ph} = \hbar\omega_\mathrm{c}\left(\hat{a}^\dagger\hat{a} + \frac{1}{2}\right) = \frac{1}{2}\left(\hat{P}_\mathrm{c}^2 + \omega_\mathrm{c}^2 \hat{Q}_\mathrm{c}^2\right), \quad \text{(A2)}$$

where ω_c is the frequency of the mode in the cavity, $\hat{a}^\dagger$ and $\hat{a}$ are the photonic creation and annihilation operators, and $\hat{Q}_\mathrm{c} = \sqrt{\hbar/2\omega_\mathrm{c}}(\hat{a}^\dagger + \hat{a})$ and $\hat{P}_\mathrm{c} = i\sqrt{\hbar\omega_\mathrm{c}/2}(\hat{a}^\dagger - \hat{a})$ are the photonic coordinate and momentum operators, respectively. Choosing the Coulomb gauge, $\nabla \cdot \hat{\mathbf{A}} = 0$, the vector potential becomes purely transverse $\hat{\mathbf{A}} = \hat{\mathbf{A}}_\perp$. Under the long-wavelength approximation,

$$\hat{\mathbf{A}} = \mathbf{A}_0\left(\hat{a} + \hat{a}^\dagger\right) = \mathbf{A}_0\sqrt{2\omega_\mathrm{c}/\hbar}\,\hat{Q}_\mathrm{c}, \quad \text{(A3)}$$

where $\mathbf{A}_0 = \sqrt{\hbar/2\omega_\mathrm{c}\varepsilon_0\mathcal{V}}\,\hat{\mathbf{e}}$, with $\mathcal{V}$ as the quantization volume inside the cavity, ε_0 as the permittivity, and $\hat{\mathbf{e}}$ as the unit vector of the field polarization.

We further introduce the Power–Zienau–Woolley (PZW) gauge transformation operator[57,114] as

$$\hat{U} = \exp\left[-\frac{i}{\hbar}\hat{\boldsymbol{\mu}}\cdot\hat{\mathbf{A}}\right] = \exp\left[-\frac{i}{\hbar}\hat{\boldsymbol{\mu}}\cdot\mathbf{A}_0\left(\hat{a} + \hat{a}^\dagger\right)\right]. \quad \text{(A4)}$$

The PZW transformation operator can also be expressed as $\hat{U} = \exp\left[-\frac{i}{\hbar}\sqrt{2\omega_\mathrm{c}/\hbar}\hat{\boldsymbol{\mu}}\mathbf{A}_0\hat{Q}_\mathrm{c}\right] = \exp\left[-\frac{i}{\hbar}\left(\sum_j z_j\hat{\mathbf{A}}\mathbf{x}_j\right)\right]$. Recall that a momentum boost operator $\hat{U}_\mathrm{p} = e^{-\frac{i}{\hbar}p_0\hat{q}}$ displaces $\hat{p}$ by the amount of p_0 such that $\hat{U}_\mathrm{p}\hat{O}(\hat{p})\hat{U}_\mathrm{p}^\dagger = \hat{O}(\hat{p} + p_0)$. Hence, $\hat{U}$ is a boost operator for both the photonic momentum $\hat{P}_\mathrm{c}$ by the amount of $\sqrt{2\omega_\mathrm{c}/\hbar}\hat{\boldsymbol{\mu}}\mathbf{A}_0$ and the matter momentum $\hat{\mathbf{P}}_j$ by the amount of $z_j\hat{\mathbf{A}}$. Using $\hat{U}^\dagger$ to boost the matter momentum, one can show that

$$\hat{H}_\mathrm{C} = \hat{U}^\dagger\hat{H}_\mathrm{m}\hat{U} + \hat{H}_\mathrm{ph}; \quad \text{(A5)}$$

hence, $\hat{H}_\mathrm{C}$ can be obtained[115] by a momentum boost with the amount of $-z_j\hat{\mathbf{A}}$ for $\hat{\mathbf{P}}_j$ and then by adding $\hat{H}_\mathrm{ph}$.

The QED Hamiltonian under the *dipole* gauge (the "d · E" form[114,116]) can be obtained by performing the PZW transformation on $\hat{H}_\mathrm{C}$ as follows:

$$\begin{aligned}\hat{H}_\mathrm{D} &= \hat{U}\hat{H}_\mathrm{C}\hat{U}^\dagger = \hat{U}\hat{U}^\dagger\hat{H}_\mathrm{m}\hat{U}\hat{U}^\dagger + \hat{U}\hat{H}_\mathrm{ph}\hat{U}^\dagger \\ &= \hat{H}_\mathrm{m} + \hbar\omega_\mathrm{c}\left(\hat{a}^\dagger\hat{a} + \frac{1}{2}\right) + i\omega_\mathrm{c}\hat{\boldsymbol{\mu}}\mathbf{A}_0(\hat{a}^\dagger - \hat{a}) + \frac{\omega_\mathrm{c}}{\hbar}(\hat{\boldsymbol{\mu}}\mathbf{A}_0)^2, \quad \text{(A6)}\end{aligned}$$

where we have used supplementary material, Eq. (23) to express $\hat{H}_\mathrm{C}$, and the last three terms of the above equation are the results of $\hat{U}\hat{H}_\mathrm{ph}\hat{U}^\dagger$. Using $\hat{Q}_\mathrm{c}$ and $\hat{P}_\mathrm{c}$, one can instead show that

$$\hat{H}_\mathrm{D} = \hat{H}_\mathrm{m} + \frac{1}{2}\omega_\mathrm{c}^2\hat{Q}_\mathrm{c}^2 + \frac{1}{2}\left(\hat{P}_\mathrm{c} + \sqrt{2\omega_\mathrm{c}/\hbar}\hat{\boldsymbol{\mu}}\mathbf{A}_0\right)^2 \quad \text{(A7)}$$

because the PZW operator boosts the photonic momentum $\hat{P}_\mathrm{c}$ by $\sqrt{2\omega_\mathrm{c}/\hbar}\hat{\boldsymbol{\mu}}\mathbf{A}_0$. The term $\frac{\omega_\mathrm{c}}{\hbar}(\hat{\boldsymbol{\mu}}\mathbf{A}_0)^2$ is commonly referred to as the dipole self-energy (DSE).

The Pauli–Fierz (PF) QED Hamiltonian[6,20,21] can be obtained by using a unitary transformation $\hat{U}_\phi = \exp[i\frac{\pi}{2}\hat{a}^\dagger\hat{a}]$ on $\hat{H}_\mathrm{D}$. To proceed, we use the following Baker–Campbell–Hausdorff (BCH) identity

$$e^{\hat{A}}\hat{B}e^{-\hat{A}} = \hat{B} + [\hat{A}, \hat{B}] + \frac{1}{2!}[\hat{A}, [\hat{A}, \hat{B}]] + \cdots \quad \text{(A8)}$$

Using the fundamental commutator $[\hat{a}^\dagger, \hat{a}] = -1$, we have $[\hat{a}^\dagger\hat{a}, \hat{a}] = \hat{a}^\dagger[\hat{a}, \hat{a}] + [\hat{a}^\dagger, \hat{a}]\hat{a} = -\hat{a}$. Denoting $\hat{U}_\phi = \exp[i\phi\hat{a}^\dagger\hat{a}] = e^{-\hat{A}}$ (with $\phi = \frac{\pi}{2}$), hence $\hat{A} = -i\phi\hat{a}^\dagger\hat{a}$. Using the BCH identity, we have

$$\begin{aligned}e^{-i\phi\hat{a}^\dagger\hat{a}}\hat{a}e^{i\phi\hat{a}^\dagger\hat{a}} &= \hat{a} - i\phi[\hat{a}^\dagger\hat{a}, \hat{a}] + \frac{1}{2!}(-i\phi)^2[\hat{a}^\dagger\hat{a}, [\hat{a}^\dagger\hat{a}, \hat{a}]] + \cdots \\ &= \left(1 + (-i\phi)(-1) + \frac{1}{2!}(-i\phi)^2(-1)^2 + \cdots\right)\hat{a} = e^{i\phi}\hat{a}\end{aligned}$$
$$\text{(A9)}$$

Similarly, we have $e^{-i\phi\hat{a}^\dagger\hat{a}}\hat{a}^\dagger e^{i\phi\hat{a}^\dagger\hat{a}} = e^{-i\phi}\hat{a}^\dagger$. Choosing $\phi = \frac{\pi}{2}$ results in $\hat{U}_\phi^\dagger\hat{a}\hat{U}_\phi \to i\hat{a}$ and $\hat{U}_\phi^\dagger\hat{a}^\dagger\hat{U}_\phi \to -i\hat{a}^\dagger$. Using these results, and applying $\hat{U}_\phi$ on $\hat{H}_\mathrm{D}$, we have the PF Hamiltonian as follows:

$$\hat{H}_{\mathrm{PF}} = \hat{U}_\phi \hat{H}_{\mathrm{D}} \hat{U}_\phi^\dagger$$

$$= \hat{H}_{\mathrm{m}} + \hbar\omega_c \left(\hat{a}^\dagger \hat{a} + \frac{1}{2} \right) + \mathbf{A}_0 \omega_c \hat{\boldsymbol{\mu}} (\hat{a} + \hat{a}^\dagger) + \frac{\omega_c}{\hbar} (\mathbf{A}_0 \hat{\boldsymbol{\mu}})^2$$

$$= \hat{H}_{\mathrm{m}} + \frac{1}{2} \hat{P}_c^2 + \frac{1}{2} \omega_c^2 \left(\hat{Q}_c + \frac{A_0 \hat{\boldsymbol{\mu}}}{\sqrt{\hbar\omega_c}} \right)^2, \qquad (A10)$$

where the coupling constant is $\frac{A_0}{\sqrt{\hbar\omega_c}} = \sqrt{\frac{2}{\hbar\omega_c^3}} \chi$ as we used in Eq. (1).

Note that we have used the fact that $\hat{U}_\phi \hat{H}_{\mathrm{m}} \hat{U}_\phi^\dagger = \hat{H}_{\mathrm{m}}$, i.e., $\hat{U}_\phi$ does not contain any matter DOFs. Hence, the role of $\hat{U}_\phi$ is to switch $\hat{P}_c$ and $\hat{Q}_c$, and for a photon field, they are inter-changeable due to the pure harmonic nature of the quantized field. The PF Hamiltonian has the advantage as a pure real Hamiltonian and the photonic DOF can be viewed[6,21] and computationally treated[26,28] as "nuclear coordinates."

In quantum optics, a two-level atom coupled to a single model in an optical cavity is a well-studied subject. This leads to the well-known model Hamiltonian, such as the Rabi model and the Jaynes–Cummings model. Since these two models are also widely used in recent investigations of polariton chemistry, here we briefly derive them from the PF Hamiltonian.

We consider a molecule with two electronic states,

$$\hat{\mathcal{H}}_{\mathrm{M}} = \hat{T} + E_g(R) |g\rangle\langle g| + E_e(R) |e\rangle\langle e|, \qquad (A11)$$

and the transition dipole is $\boldsymbol{\mu}_{eg} = \langle e|\hat{\boldsymbol{\mu}}|g\rangle$. Note that the permanent dipoles in a molecule $\boldsymbol{\mu}_{ee} = \langle e|\hat{\boldsymbol{\mu}}|e\rangle$, $\boldsymbol{\mu}_{gg} = \langle g|\hat{\boldsymbol{\mu}}|g\rangle$ are not necessarily zero, as opposed to the atomic case where they are always zero. Hence, it is not always a good approximation to drop them.

The Rabi model assumes that one can drop the permanent dipoles and leads to the dipole operator expression in the subspace $\hat{\mathcal{P}} = |g\rangle\langle g| + |e\rangle\langle e|$ as follows:

$$\hat{\mathcal{P}} \hat{\boldsymbol{\mu}} \hat{\mathcal{P}} = \boldsymbol{\mu}_{eg} (|e\rangle\langle g| + |g\rangle\langle e|) \equiv \boldsymbol{\mu}_{eg} (\hat{\sigma}^\dagger + \hat{\sigma}), \qquad (A12)$$

where we have defined the creation operator $\hat{\sigma}^\dagger \equiv |e\rangle\langle g|$ and annihilation operator $\hat{\sigma} \equiv |g\rangle\langle e|$ of the electronic excitation. The PF Hamiltonian [Eq. (A10)] in the subspace $\hat{\mathcal{P}}$ thus becomes

$$\hat{\mathcal{H}}_{\mathrm{PF}} = \hat{\mathcal{H}}_{\mathrm{M}} + \hat{H}_{\mathrm{ph}} + \chi \cdot \boldsymbol{\mu}_{eg} (\hat{\sigma}^\dagger + \hat{\sigma})(\hat{a}^\dagger + \hat{a}) + \frac{(\chi \cdot \boldsymbol{\mu}_{eg})^2}{\hbar\omega_c}. \qquad (A13)$$

Dropping the DSE (the last term) from Eq. (A13) leads to the Rabi model

$$\hat{\mathcal{H}}_{\mathrm{Rabi}} = \hat{\mathcal{H}}_{\mathrm{M}} + \hat{H}_{\mathrm{ph}} + \chi \cdot \boldsymbol{\mu}_{eg} (\hat{\sigma}^\dagger + \hat{\sigma})(\hat{a}^\dagger + \hat{a}). \qquad (A14)$$

Dropping both the DSE and the counter-rotating terms $\hat{\sigma}^\dagger \hat{a}^\dagger$ and $\hat{\sigma}\hat{a}$ leads to the well-known Jaynes–Cummings model[117] as follows:

$$\hat{\mathcal{H}}_{\mathrm{JC}} = \hat{\mathcal{H}}_{\mathrm{M}} + \hat{H}_{\mathrm{ph}} + \chi \cdot \boldsymbol{\mu}_{eg} (\hat{\sigma}^\dagger \hat{a} + \hat{\sigma}\hat{a}^\dagger). \qquad (A15)$$

The limitations of these two models are thoroughly discussed in our recent work on PMET[58] and polariton mediated photodissociation dynamics for diatomic molecules.[22]

DATA AVAILABILITY

The data that support the findings of this study are available from the corresponding author upon reasonable request.

REFERENCES

[1] J. A. Hutchison, T. Schwartz, C. Genet, E. Devaux, and T. W. Ebbesen, Angew. Chem., Int. Ed. **51**, 1592 (2012).

[2] A. Thomas, L. Lethuillier-Karl, K. Nagarajan, R. M. A. Vergauwe, J. George, T. Chervy, A. Shalabney, E. Devaux, C. Genet, J. Moran, and T. W. Ebbesen, Science **363**, 615 (2019).

[3] A. Thomas, A. Jayachandran, L. Lethuillier-Karl, R. M. A. Vergauwe, K. Nagarajan, E. Devaux, C. Genet, J. Moran, and T. W. Ebbesen, Nanophotonics **9**, 249 (2020).

[4] M. Kowalewski, K. Bennett, and S. Mukamel, J. Phys. Chem. Lett. **7**, 2050 (2016).

[5] J. Galego, C. Climent, F. J. Garcia-Vidal, and J. Feist, Phys. Rev. X **9**, 021057 (2019).

[6] C. Schäfer, M. Ruggenthaler, and A. Rubio, Phys. Rev. A **98**, 043801 (2018).

[7] K. Bennett, M. Kowalewski, and S. Mukamel, Faraday Discuss. **194**, 259 (2016).

[8] F. Herrera and F. C. Spano, Phys. Rev. Lett. **116**, 238301 (2016).

[9] M. Kowalewski, K. Bennett, and S. Mukamel, J. Chem. Phys. **144**, 054309 (2016).

[10] J. Feist, J. Galego, and F. J. Garcia-Vidal, ACS Photonics **5**, 205 (2018).

[11] J. F. Triana, D. Peláez, and J. L. Sanz-Vicario, J. Phys. Chem. A **122**, 2266 (2018).

[12] J. Fregoni, G. Granucci, E. Coccia, M. Persico, and S. Corni, Nat. Commun. **9**, 4688 (2018).

[13] O. Vendrell, Chem. Phys. **509**, 55 (2018).

[14] B. Gu and S. Mukamel, Chem. Sci. **11**, 1290 (2020).

[15] A. Mandal and P. Huo, J. Phys. Chem. Lett. **10**, 5519 (2019).

[16] A. Csehi, M. Kowalewski, G. J. Halász, and Á. Vibók, New J. Phys. **21**, 093040 (2019).

[17] T. Szidarovszky, G. J. Halász, A. G. Császár, L. S. Cederbaum, and Á. Vibók, J. Phys. Chem. Lett. **9**, 6215 (2018).

[18] G. Groenhof and J. J. Toppari, J. Phys. Chem. Lett. **9**, 4848 (2018).

[19] G. Groenhof, C. Climent, J. Feist, D. Morozov, and J. J. Toppari, J. Phys. Chem. Lett. **10**, 5476 (2019).

[20] V. Rokaj, D. M. Welakuh, M. Ruggenthaler, and A. Rubio, J. Phys. B: At. Mol. Opt. Phys. **51**, 034005 (2018).

[21] J. Flick, M. Ruggenthaler, H. Appel, and A. Rubio, Proc. Natl. Acad. Sci. U. S. A. **114**, 3026 (2017).

[22] A. Mandal, S. Montillo Vega, and P. Huo, J. Phys. Chem. Lett. **11**, 9215–9223 (2020).

[23] W. H. Miller, J. Chem. Phys. **69**, 2188 (1978).

[24] A. E. Orel and W. H. Miller, J. Chem. Phys. **70**, 4393 (1979).

[25] N. M. Hoffmann, C. Schäfer, A. Rubio, A. Kelly, and H. Appel, Phys. Rev. A **99**, 063819 (2019).

[26] N. M. Hoffmann, C. Schäfer, N. Säkkinen, A. Rubio, H. Appel, and A. Kelly, J. Chem. Phys. **151**, 244113 (2019).

[27] N. M. Hoffmann, L. Lacombe, A. Rubio, and N. T. Maitra, J. Chem. Phys. **153**, 104103 (2020).

[28] T. E. Li, H.-T. Chen, A. Nitzan, and J. E. Subotnik, Phys. Rev. A **101**, 033831 (2020).

[29]S. Habershon and D. E. Manolopoulos, J. Chem. Phys. **131**, 244518 (2009).

[30]U. Müller and G. Stock, J. Chem. Phys. **111**, 77 (1999).

[31]S. N. Chowdhury and P. Huo, J. Chem. Phys. **150**, 244102 (2019).

[32]H.-T. Chen, T. E. Li, A. Nitzan, and J. E. Subotnik, Phys. Rev. A **100**, 010101(R) (2019).

[33]J. O. Richardson and M. Thoss, J. Chem. Phys. **139**, 031102 (2013).

[34]T. J. H. Hele and N. Ananth, Faraday Discuss. **195**, 269 (2016).

[35]N. Ananth, J. Chem. Phys. **139**, 124102 (2013).

[36]J. R. Duke and N. Ananth, J. Phys. Chem. Lett. **6**, 4219 (2015).

[37]S. Pierre, J. R. Duke, T. J. H. Hele, and N. Ananth, J. Chem. Phys. **147**, 234103 (2017).

[38]J. O. Richardson, P. Meyer, M.-O. Pleinert, and M. Thoss, Chem. Phys. **482**, 124 (2017).

[39]B. J. Berne and D. Thirumalai, Annu. Rev. Phys. Chem. **37**, 401 (1986).

[40]D. M. Ceperley, Rev. Mod. Phys. **67**, 279 (1995).

[41]D. Chandler and P. G. Wolynes, J. Chem. Phys. **74**, 4078 (1981).

[42]J. Cao and G. A. Voth, J. Chem. Phys. **100**, 5106 (1994).

[43]I. R. Craig and D. E. Manolopoulos, J. Chem. Phys. **121**, 3368 (2004).

[44]S. Habershon, D. E. Manolopoulos, T. E. Markland, and T. F. Miller, Annu. Rev. Phys. Chem. **64**, 124105 (2013).

[45]D. F. Coker, B. J. Berne, and D. Thirumalai, J. Chem. Phys. **86**, 5689 (1987).

[46]A. R. Menzeleev and T. F. Miller, J. Chem. Phys. **132**, 034106 (2010).

[47]A. R. Menzeleev, N. Ananth, and T. F. Miller, J. Chem. Phys. **135**, 074106 (2011).

[48]C. G. Bischak, C. L. Hetherington, H. Wu, S. Aloni, D. F. Ogletree, D. T. Limmer, and N. S. Ginsberg, Nano Lett. **17**, 1028 (2017).

[49]R. Collepardo-Guevara, I. R. Craig, and D. E. Manolopoulos, J. Chem. Phys. **128**, 144502 (2008).

[50]A. Pérez, M. E. Tuckerman, H. P. Hjalmarson, and O. A. von Lilienfeld, J. Am. Chem. Soc. **132**, 11510 (2010).

[51]N. Boekelheide, R. Salomón-Ferrer, and T. F. Miller III, Proc. Natl. Acad. Sci. U. S. A. **108**, 16159 (2011).

[52]T. E. Markland, S. Habershon, and D. E. Manolopoulos, J. Chem. Phys. **128**, 194506 (2008).

[53]T. F. Miller and D. E. Manolopoulos, J. Chem. Phys. **122**, 184503 (2005).

[54]J. S. Kretchmer and T. F. Miller, J. Chem. Phys. **138**, 134109 (2013).

[55]J. S. Kretchmer and T. F. Miller, Inorg. Chem. **55**, 1022 (2016).

[56]R. C. Remsing and J. E. Bates, J. Chem. Phys. **153**, 121104 (2020).

[57]C. Cohen-Tannoudji, J. Dupont-Roc, and G. Grynberg, "Photons and atoms, introduction to quantum electrodynamics" (John Wiley & Sons, Inc., Hoboken, USA, 1989).

[58]A. Mandal, T. D. Krauss, and P. Huo, J. Phys. Chem. B **124**, 6321 (2020).

[59]J. George, T. Chervy, A. Shalabney, E. Devaux, H. Hiura, C. Genet, and T. W. Ebbesen, Phys. Rev. Lett. **117**, 153601 (2016).

[60]H. D. Meyer and W. H. Miller, J. Chem. Phys. **70**, 3214 (1979).

[61]G. Stock and M. Thoss, Phys. Rev. Lett. **78**, 578 (1997).

[62]A. Semenov and A. Nitzan, J. Chem. Phys. **150**, 174122 (2019).

[63]J. A. Campos-Gonzalez-Angulo, R. F. Ribeiro, and J. Yuen-Zhou, Nat. Commun. **10**, 4685 (2019).

[64]W. Xie, S. Bai, L. Zhu, and Q. Shi, J. Phys. Chem. A **117**, 6196 (2013).

[65]X. Sun and E. Geva, J. Chem. Phys. **144**, 044106 (2016).

[66]X. Sun and E. Geva, J. Chem. Phys. **144**, 244105 (2016).

[67]X. Sun and E. Geva, J. Phys. Chem. A **120**, 2976 (2016).

[68]A. A. Kananenka, X. Sun, A. Schubert, B. D. Dunietz, and E. Geva, J. Chem. Phys. **148**, 102304 (2018).

[69]X. Sun and E. Geva, J. Chem. Theory Comput. **12**, 2926 (2016).

[70]X. Sun and E. Geva, J. Chem. Phys. **145**, 064109 (2016).

[71]Z. Hu, Z. Tong, M. S. Cheung, B. D. Dunietz, E. Geva, and X. Sun, J. Phys. Chem. B **124**, 9579 (2020).

[72]Z. Tong, X. Gao, M. S. Cheung, B. D. Dunietz, E. Geva, and X. Sun, J. Chem. Phys. **153**, 044105 (2020).

[73]R. A. Marcus, J. Chem. Phys. **24**, 966 (1956).

[74]A. Nitzan, J. Jortner, P. M. Rentzepis, and G. Porter, Proc. R. Soc. Lond. A **327**, 367–391 (1972).

[75]J. Ulstrup and J. Jortner, J. Chem. Phys. **63**, 4358 (1975).

[76]S. Efrima and M. Bixon, Chem. Phys. Lett. **25**, 34 (1974).

[77]W. B. Davis, M. A. Ratner, and M. R. Wasielewski, J. Am. Chem. Soc. **123**, 7877 (2001).

[78]D. N. Beratan, J. N. Onuchic, and J. J. Hopfield, J. Chem. Phys. **86**, 4488 (1987).

[79]D. N. Beratan and J. N. Onuchic, Photosynth. Res. **22**, 173 (1989).

[80]J. N. Onuchic and D. N. Beratan, J. Chem. Phys. **92**, 722 (1990).

[81]A. Troisi, A. Nitzan, and M. A. Ratner, J. Chem. Phys. **119**, 5782 (2003).

[82]S. S. Skourtis, D. H. Waldeck, and D. N. Beratan, Annu. Rev. Phys. Chem. **61**, 461 (2010).

[83]P. Antoniou, Z. Ma, P. Zhang, D. N. Beratan, and S. S. Skourtis, Phys. Chem. **17**, 30854–30866 (2015).

[84]I. A. Goychuk, E. G. Petrov, and V. May, J. Chem. Phys. **103**, 4937 (1995).

[85]D. N. Beratan, S. S. Skourtis, I. A. Balabin, A. Balaeff, S. Keinan, R. Venkatramani, and D. Xiao, Acc. Chem. Res. **42**, 1669 (2009).

[86]T. R. Prytkova, I. V. Kurnikov, and D. N. Beratan, Science **315**, 622 (2007).

[87]J. Antony, D. M. Medvedev, and A. A. Stuchebrukhov, J. Am. Chem. Soc. **122**, 1057 (2000).

[88]E. S. Medvedev and A. A. Stuchebrukhov, J. Chem. Phys. **107**, 3821 (1997).

[89]I. Daizadeh, E. S. Medvedev, and A. A. Stuchebrukhov, Proc. Natl. Acad. Sci. U. S. A. **94**, 3703 (1997).

[90]Z. Ma, Z. Lin, C. M. Lawrence, I. V. Rubtsov, P. Antoniou, S. S. Skourtis, P. Zhang, and D. N. Beratan, Chem. Sci. **9**, 6395 (2018).

[91]A. Jain and J. E. Subotnik, J. Phys. Chem. Lett. **6**, 4809 (2015).

[92]A. Jain and J. E. Subotnik, J. Chem. Phys. **143**, 134107 (2015).

[93]S. J. Cotton and W. H. Miller, J. Chem. Phys. **150**, 104101 (2019).

[94]W. H. Miller and S. J. Cotton, J. Chem. Phys. **145**, 081102 (2016).

[95]W. H. Miller, S. D. Schwartz, and J. W. Tromp, J. Chem. Phys. **79**, 4889 (2009).

[96]R. A. Marcus and N. Sutin, Biochim. Biophys. Acta, Biophys. Incl. Photsynth. **811**, 265 (1985).

[97]S. Hammes-Schiffer and A. A. Stuchebrukhov, Chem. Rev. **110**, 6939 (2010).

[98]S. Hammes-Schiffer, Energy Environ. Sci. **5**, 7696 (2012).

[99]J. R. Duke and N. Ananth, Faraday Discuss. **195**, 253 (2016).

[100]J. Liu and W. H. Miller, J. Chem. Phys. **134**, 104101 (2011).

[101]N. Renaud and F. C. Grozema, J. Phys. Chem. Lett. **6**, 360 (2015).

[102]J. Aragó and A. Troisi, Phys. Rev. Lett. **114**, 026402 (2015).

[103]M. A. Castellanos and P. Huo, J. Phys. Chem. Lett. **8**, 2480 (2017).

[104]A. F. Kockum, A. Miranowicz, S. D. Liberato, S. Savasta, and F. Nori, Nat. Rev. **1**, 19 (2019).

[105]J. del Pino, F. A. Y. N. Schröder, A. W. Chin, J. Feist, and F. J. Garcia-Vidal, Phys. Rev. Lett. **121**, 227401 (2018).

[106]S. N. Chowdhury and P. Huo, J. Chem. Phys. **147**, 214109 (2017).

[107]A. R. Menzeleev, F. Bell, and T. F. Miller, J. Chem. Phys. **140**, 064103 (2014).

[108]J. S. Kretchmer, N. Boekelheide, J. J. Warren, J. R. Winkler, H. B. Gray, and T. F. Miller, Proc. Natl. Acad. Sci. U. S. A. **115**, 6129 (2018).

[109]S. Jang and G. A. Voth, J. Chem. Phys. **111**, 2371 (1999).

[110]J.-L. Liao and G. A. Voth, J. Phys. Chem. B **106**, 8449 (2002).

[111]B. F. E. Curchod and T. J. Martínez, Chem. Rev. **118**, 3305 (2018).

[112]G. W. Richings, I. Polyak, K. E. Spinlove, G. A. Worth, I. Burghardt, and B. Lasorne, Int. Rev. Phys. Chem. **34**, 269 (2015).

[113]T. W. Ebbesen, Acc. Chem. Res. **49**, 2403 (2016).

[114]E. A. Power and S. Zienau, Philos. Trans. R. Soc., A **251**, 427 (1959).

[115]O. D. Stefano, A. Settineri, V. Macri, L. Garziano, R. Stassi, S. Savasta, and F. Nori, Nat. Phys. **15**, 803 (2019).

[116]M. Göppert-Mayer, Ann. Phys. (Berlin) **18**, 466 (2009).

[117]E. T. Jaynes and F. W. Cummings, Proc. IEEE **51**, 89–109 (1963).